AIP | Review of Scientific Instruments

# A large electrochemical setup for the anodization of aluminum towards highly ordered arrays of cylindrical nanopores

Loïc Assaud, Sebastian Bochmann, Silke Christiansen, and Julien Bachmann

Citation: Review of Scientific Instruments **86**, 073902 (2015); doi: 10.1063/1.4926746
View online: http://dx.doi.org/10.1063/1.4926746
View Table of Contents: http://scitation.aip.org/content/aip/journal/rsi/86/7?ver=pdfcov
Published by the AIP Publishing



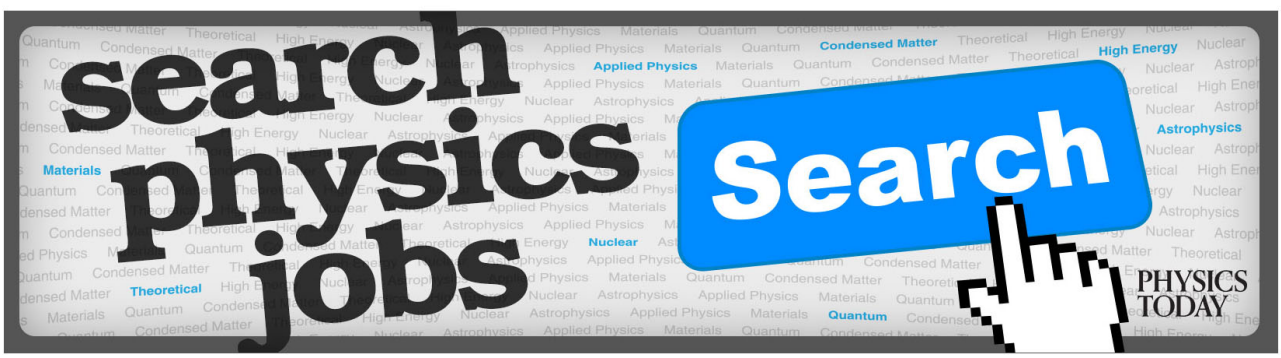

# A large electrochemical setup for the anodization of aluminum towards highly ordered arrays of cylindrical nanopores

Loïc Assaud,[1,a),b)] Sebastian Bochmann,[1] Silke Christiansen,[2] and Julien Bachmann[1,a)]
[1]*Department of Chemistry and Pharmacy, Friedrich-Alexander University Erlangen-Nürnberg, Egerlandstrasse 1, 91058 Erlangen, Germany*
[2]*Max Planck Institute for the Science of Light, Günther-Scharowsky-Strasse 1, 91058 Erlangen, Germany and Helmholtz-Center Berlin (HZB), Hahn-Meitner-Platz 1, 14109 Berlin, Germany*

(Received 11 December 2014; accepted 1 July 2015; published online 15 July 2015)

A new electrochemical setup and the associated procedures for growing ordered anodic aluminum oxide pore arrays on large surfaces are presented. The typical size of the samples is $14 \times 14$ cm$^2$. The most crucial experimental parameters that allow for the stabilization of the high-field procedures are a very efficient cooling of sample and electrolyte, as well as the initial ramping up of the voltage at an accurately defined rate. The morphology of the cylindrical, parallel alumina pores is similar to those obtained on smaller scales with standard setups. Our setup facilitates the availability of porous anodic alumina as a template system for a number of applications. © *2015 AIP Publishing LLC.* [http://dx.doi.org/10.1063/1.4926746]

## I. INTRODUCTION

Nanoporous, ordered "anodic" oxide membranes appear, as substrates or templates, in numerous applications such as filtration, biology, energy storage, and catalysis.[1–10] The unique features of anodic oxide systems are the parallel, cylindrical pores, their high aspect ratios, and the wide tunability of their geometric parameters. Correspondingly, much attention has been dedicated to the fabrication of those nanostructured systems, in particular, $TiO_2$ and $Al_2O_3$,[11–14] both from the fundamental mechanistic viewpoint and in terms of its practical implementation. To date, most anodic oxide templates, both commercially available ones and academic, typically more highly ordered, ones, are of limited size (on the order of several mm$^2$ or cm$^2$).[15] In particular, no setup for the anodization of aluminum in phosphoric acid at >190 V over significantly more than 10 cm$^2$ has been available. The setup presented in this paper fills this gap.

The electrochemical nanostructuration of alumina surfaces was first performed in the early 1950s,[16,17] followed by a significant expansion of its academic utilization with the discovery by Masuda and Fukuda of the self-organization of alumina membranes using the so-called two-step anodization process in 1996.[18] The porous anodic aluminum oxide (AAO) obtained after high-field anodization consists of a thin, continuous barrier oxide layer supported on an aluminum substrate, surmounted by cylindrical, parallel nanopores. The pores are organized according to a hexagonal arrangement. Under a number of distinct sets of specific electrochemical conditions, determined by the acidic medium, the temperature, and the applied potential, a self-organization of the pores takes place, leading to a highly ordered array of pores.[19–28] Crucial to the success of a steady-state, self-ordering anodization is the accurate control of the temperature. Insufficient cooling generates a catastrophic local temperature increase due to Joule heating and ultimately leads to pitting.[29] This design requirement has been the major factor limiting scale-up of electrochemical setups for the anodic generation of highly ordered nanoporous systems.

In the present paper, we report on the development of a new anodization setup which is able to grow AAO membranes on surfaces of up to $14 \times 14$ cm$^2$ and in the two most important sets of conditions: 195 V in $H_3PO_4$ (yielding pores of 180 nm diameter and 450 nm pitch) and 40 V in $H_2C_2O_4$ (yielding pores of 40 nm diameter and 105 nm pitch). The setup and their different components are described and the morphology of alumina pores is characterized by electron microscopy. The advances of our setup with respect to previously described setups in the literature are the following: (1) more efficient removal of the reaction heat and better control of the reaction temperature via simultaneous cooling of the anode and the electrolyte, (2) improved homogeneity of the electrolyte motion via an externally circulated electrolyte instead of stirring, (3) control of the initial stages of pore formation via potential ramping. These three aspects are the crucial parameters that allow for a homogeneous anodization without catastrophic pitting on a large area.

## II. SHORT SUMMARY OF A GENERAL ANODIZATION PROCEDURE

The growth of alumina pores occurs in acidic electrolytes such as sulfuric, oxalic, and phosphoric.[30] Neutral electrolytes result in a non-porous layer of aluminum oxide. In contrast to this, acids may lead to a localized dissolution of the aluminum oxide layer. In the traditional model, locally enhanced ion conduction due to the high electric field supports this dissolution, which results in the growth of pores as the metal/oxide interface moves into the metal bulk.[31,32] More recent models

a)Authors to whom correspondence should be addressed. Electronic addresses: loic.assaud@fau.de and julien.bachmann@fau.de
b)Current address: Université Paris-Sud, CNRS, Institut de Chimie Moléculaire et des Matériaux d'Orsay, Rue du Doyen Georges Poitou, 91400 Orsay, France.

 

TABLE I. Standard anodization parameters reported in the literature.[30]

| $D$ (nm) | $D_c$ (nm) | $U$ (V) | Acid | $T$ (°C) |
|---|---|---|---|---|
| 25 | 65 | 25 | $H_2SO_4$ | 10 |
| 35 | 105 | 40 | $H_2C_2O_4$ | 8 |
| 180 | 450 | 195 | $H_3PO_4$ | 2 |

also consider other aspects, such as the mechanical effects on ion mobility inside the oxide layer.[33,34] The pores self-order due to the volume expansion taking place when Al is converted to $Al_2O_3$. This expansion causes a mechanical stress which is best released in an ordered system of pores. Based on this general principle, a large variety of pore sizes can be defined in the aluminum/alumina system, depending on the applied voltage and the nature of the electrolyte. The diameter $D$ and the pitch $D_c$ are directly proportional to the applied anodization voltage $U$,[30]

$$D = \lambda \times U,$$
$$D_c = \lambda_c \times U,$$

where the proportionality constants are empirically found to be $\lambda \approx 0.95$ nm/V and $\lambda_c \approx 2.5$ nm/V. Standard sets of parameters found in the literature are provided in Table I.

In practice, pores are initiated at surface irregularities present initially, and they only order as they grow. The undesired presence of a disordered layer is circumvented by a two-step procedure as summarized in Fig. 1. A homogeneously planar surface is necessary as a starting material to reach a well-ordered pore array. Thus, the commercial Al foil (Fig. 1(a)) is first electropolished in an acidic solution to obtain a mirror-like substrate (Fig. 1(b)). A first anodization step leads to an inhomogeneous alumina layer of pores (Fig. 1(c)) which is chemically dissolved subsequently. The resulting prestructured Al surface (Fig. 1(d)) is then anodized again. The pores start to grow from the hemispherical indentations, yielding an organized alumina membrane (Fig. 1(e)).

## III. ANODIZATION SETUP

A scheme of the electrochemical cell is presented in Fig. 2. The volume containing the electrolytic solution is defined by a poly(vinyl chloride) (PVC) frame (1) of $17 \times 17$ cm$^2$ lateral size and 2 cm thickness held between two plate electrodes. The technical drawing of the PVC frame is provided in Fig. 3. This part features two fluorocarbonate rubber (Viton®) O-rings on

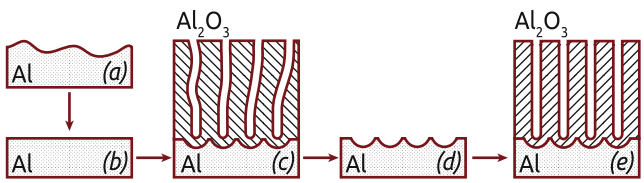


FIG. 1. Schematic of alumina pores growth. (a) Al foil, (b) Al foil after electropolishing, (c) sacrificial alumina porous layer obtained after the 1st anodization step, (d) Al prestructuring after alumina removal, and (e) perfectly ordered alumina pores array obtained after the 2nd anodization step.

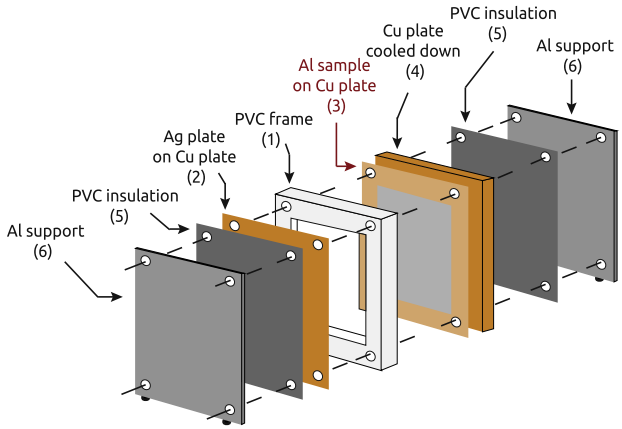


FIG. 2. Scheme representing the electrochemical cell. The Al sample and Ag counter-electrode are maintained on a Cu plate.

either sides as seals. The cathode is a thin (0.5 mm) Ag plate (2) glued on a 1-mm thick Cu plate with electrically conductive Ag glue. The Al sample (99.99% from SmartMembranes, 0.5 mm thick, cut to $14 \times 14$ cm$^2$) serving as anode is maintained on a 1-mm thick Cu plate (3) by polyamid (Kapton®) tape. Kapton is acid resistant and it ensures a good electrical insulation. This sample plate is then fixed against a cooled Cu plate (4). This central unit is surrounded on both sides by thin PVC plates (5). Aluminum alloy plates (6) close the full setup and are pressed together by screws and bolts. The four screws must be insulated by cylindrical PVC mantles in order to prevent them from getting in contact with the electrodes.

Fig. 4 shows a photograph of the open electrochemical cell. The size of the cell is $17 \times 17$ cm$^2$. The Al sample is visible at the center, as well as the Kapton tape that maintains it and insulates its edges.

Two distinct circuits are used to cool the sample and the electrolyte efficiently. Sample cooling is performed from the underlying Cu contact, which features a serpentine as sketched in Fig. 5. This serpentine is connected to a recirculating chiller delivering a cooling power of 1000 W (at 0 °C) and using a glycol fluid. The corresponding tube connections are visible in Fig. 4. In addition to this, the electrolyte is cooled separately and directly in a dedicated recirculating chiller adapted to open systems and delivering a cooling power of 550 W (at 0 °C). The corresponding tubes are connected to openings in the PVC frames (defined in Fig. 3), as observed on the photograph of

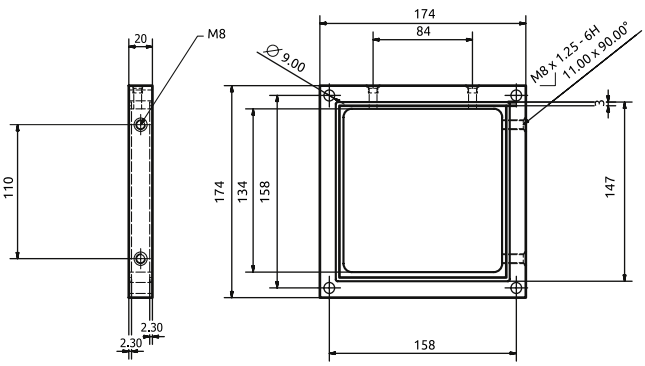


FIG. 3. Technical design of the PVC frame, part (1) in Fig. 2.

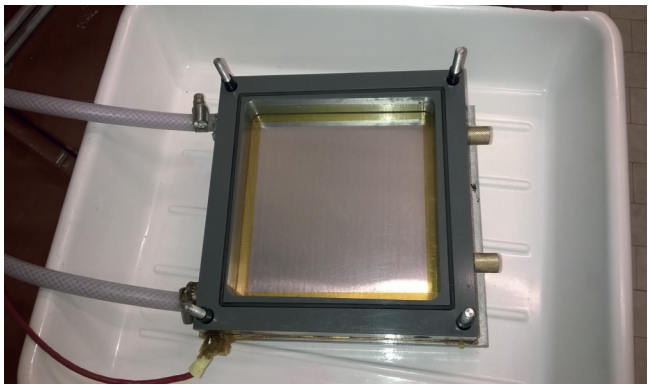

FIG. 4. Photograph of the open electrochemical cell. The main frame is made of PVC. The Al sample visible at the center is maintained on a Cu plate by Kapton tape.

the closed cell, Fig. 6. This recirculating chiller also serves to stir the electrolyte. We have used chillers from Huber and Lauda for these two purposes, whereby the former has proven unreliable in our hands. We have found quick-connect couplings on the cooling circuit to be practically useful. Additional openings in the PVC frame (shown in Figs. 3, 4, and 6) can be used to fill the system with electrolyte, to monitor the temperature of the electrolyte with a Pt100 thermoelement (protected by a PVC sheath), or can be sealed using brass caps. The Pt100 element is read by a PeakTech 5115 m.

The copper plates supporting the Al foil and the Ag plates, that is, the electrodes, are provided with electrical contacts. The system is connected to a computer-controlled power supply from EA Elektro-Automatik, such as an EA-PS 2342-06B (delivering 42 V DC / 6 A), an EA-PS 8032-20 T (32 V DC / 20 A), or an EA-PS 8360-10 T (360 V DC / 10 A), depending on exactly which step of the anodization procedure is performed. The power supplies controlled using a LabVIEW software allow the user to define voltage ramps and set the duration of the anodization. *Caution*: Care must be taken to insulate all metal parts under voltage in order to prevent short circuits and electrocution!

## IV. ANODIZATION PROCEDURE

All processing steps described in Fig. 1 can be performed in this scaled-up anodization setup. We will describe the electropolishing step, which must be performed before the anodization itself, as well as the method for obtaining two standard types of pores: those with 40 nm diameter in oxalic acid electrolyte and those with 180 nm diameter in phosphoric acid electrolyte. For the procedures described below, standard chemicals were purchased from Sigma Aldrich or VWR and used as received, whereas water was purified in a Millipore Direct-Q system. All solutions (electropolishing electrolyte, phosphoric, and oxalic acid electrolytes, as well as chromic acid) can be utilized several times.

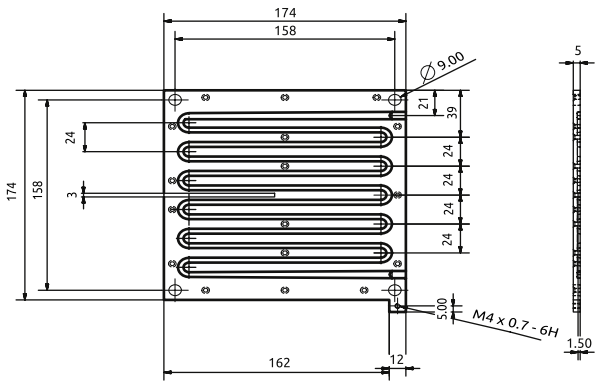


FIG. 5. Technical design of the copper cooling plate, part (4) in Fig. 2.

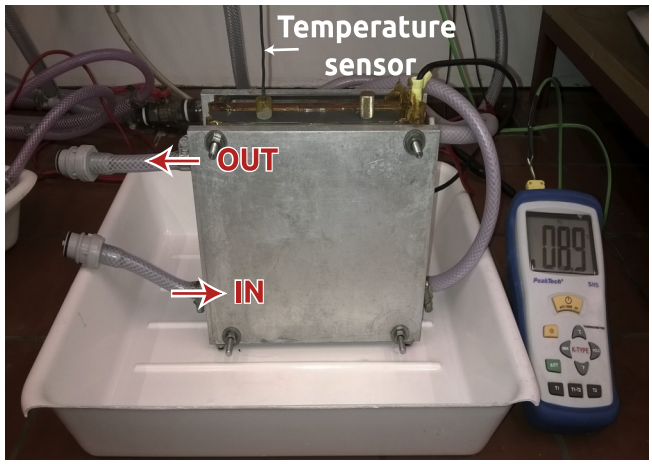


FIG. 6. Photograph of electrochemical cell prepared for the anodization step. The tubes located on the left-hand side (labeled IN and OUT) are to be connected to the electrolyte recirculating chiller, whereas the connections of the main copper plate's cooling circuit are situated on the right-hand side. The temperature is continuously monitored during the process.

### A. Electropolishing

The electropolishing is performed in ethanol/$HClO_4$ (3:1) electrolyte under 20 V. The electrolyte is neither cooled directly nor stirred. However, the Cu cooling plate underneath the Al sample is cooled to 5 °C (value set on the chiller). The electrochemical setup is put together; then, three of the four openings in the PVC frame are sealed with brass caps. The fourth opening is used to fill the volume separating the electrodes with cold electrolyte (at 5 °C approximately); then, it is used to connect an open segment of tubing that allows for volume expansion. After application of the voltage, the current stabilizes between 1.3 and 1.5 A. In order to obtain a mirror-like surface, this polishing is carried out for 45 min.

A perfect homogeneity of the electropolished sample is obtained after repeating the procedure a second time with rotated sample. For this, the electrolyte is drained, the setup is opened and rinsed with water, and then the setup is assembled again after the Al plate has been rotated by 180°. Fig. 7 shows the Al sample on its underlying copper plate before (Fig. 7(a)) and after (Fig. 7(b)) electropolishing.

### B. Anodization in oxalic acid

After draining the electropolishing solution and rinsing abundantly with water, the sample is ready to be anodized to an AAO membrane. The setup is connected to the chiller, which

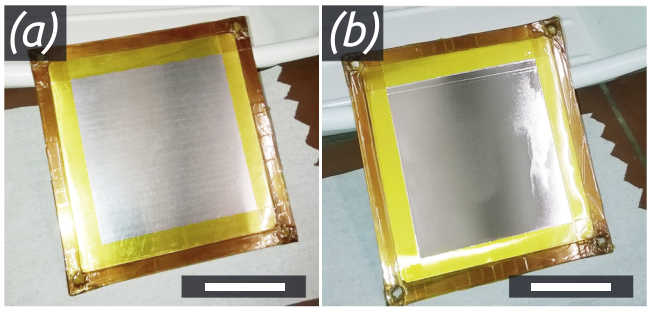


FIG. 7. Al sample maintained on the Cu plate before (a) and after (b) the electropolishing step. Scale bar: 5 cm.

circulates an aqueous 0.3 M oxalic acid solution adjusted to 5 °C (set on the chiller). The copper plate is cooled down to 5 °C (chiller setpoint). The accurate control of the temperature is the key to preventing a runaway heating up during anodization that would damage the sample.

The initial stages of anodization are the most prone to catastrophic pitting, since the initially very thin oxide layer must be thickened before the electrochemical reaction reaches the steady state. Therefore, we increase the applied voltage from 0 V with a controlled ramp, an approach that has been employed successfully in the past.[35] A starting ramp of 0.5 V/s with a compliance current of 0.8 A is applied during the first anodization up to 40 V. Subsequently, the voltage is then maintained for 22 h. At the steady state, the current is approximately 0.2-0.3 A and the temperature of the electrolyte stabilizes at 8 °C.

This first anodization is followed by a chemical dissolution of the sacrificial alumina layer in a 2% chromic acid solution in $H_3PO_4$ at 45 °C for 15 h. For this step, the Al plate must be removed from the electrochemical setup and placed in a crystallizing dish in an oven. An Al sample with prestructured surface results.

The final sample is obtained after a second anodization is carried out in the same temperature conditions as the first.

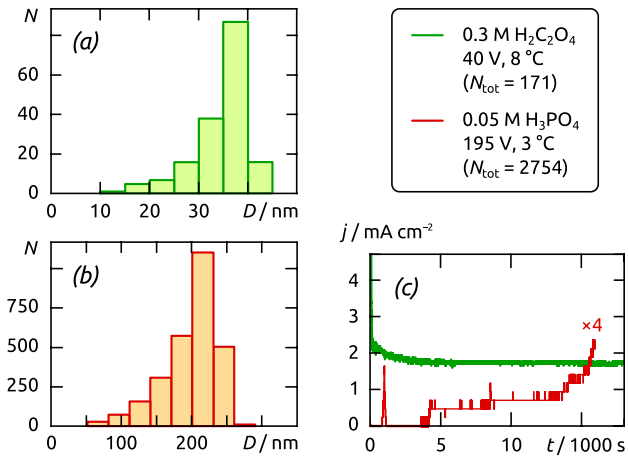


FIG. 8. Quantitative characterization of the anodization procedures: pore size distributions determined from scanning electron micrograph (SEM) image analysis for anodization in oxalic acid (a) and phosphoric acid (b), and current-time traces recorded for the second anodization step in oxalic and phosphoric acids (c), whereby the latter trace was scaled by a factor of 4. $N_{tot}$ describes the total number of pores considered in the statistical treatment.

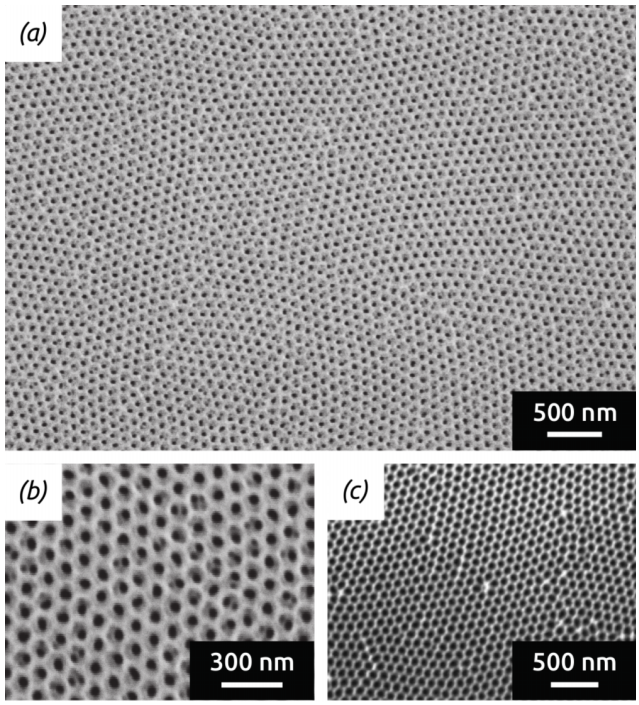


FIG. 9. (a) Scanning electron micrograph of an alumina membrane grown in 0.3 M oxalic acid under an applied potential of 40 V at 8 °C, after 5 min pore widening. (b) Enlarged view of the same sample. (c) View of a sample without pore widening.

Here, the initial voltage ramp is performed at 2 V/s from 0 to 40 V. A too fast ramp risks leading to catastrophic pitting. Conversely, if the ramp is too slow, the prestructured surface is lost and the sample displays low order. The current then reaches its final, stable value after approximately an hour, as shown in Fig. 8(c). The duration of the second anodization can be set according to the desired pore length. A growth rate of 3 $\mu$m/h has been determined empirically.

The sample is removed from the electrochemical setup and rinsed. At this point, most pores have a diameter between 35 nm and 40 nm (Fig. 8(a)), whereas a Gaussian fit of the data delivers 37(±2) nm as the mean and $2\sigma$ interval of the distribution. These values are in good agreement with the literature reports based on smaller anodization setups (Table I).[30] The diameter of the pores can optionally be increased by a subsequent thermal isotropic etching at 45 °C in 5 wt. % phosphoric acid solution. The etching rate is approximately 1 nm/min. Fig. 9 shows alumina pores resulting from the

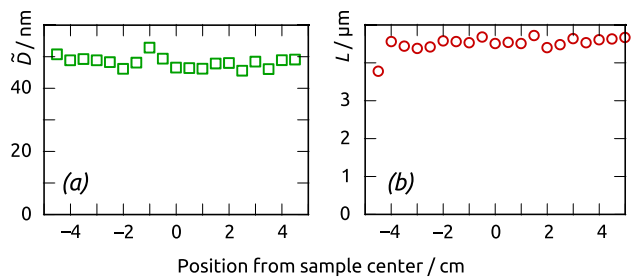


FIG. 10. Homogeneity of the nanopore geometry over a sample of approximately 10 cm lateral size. The graphs show (a) the average pore diameter (assessed by digital image processing) and (b) the pore length at various points from one edge of the sample to the other.

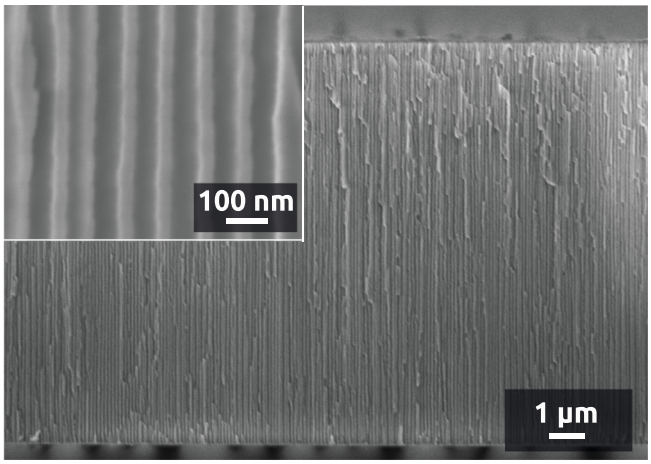


FIG. 11. Cross-sectional view of an alumina membrane grown in 0.3 M oxalic acid under an applied potential of 40 V at 8 °C. The inset shows an enlarged view of the pores' section.

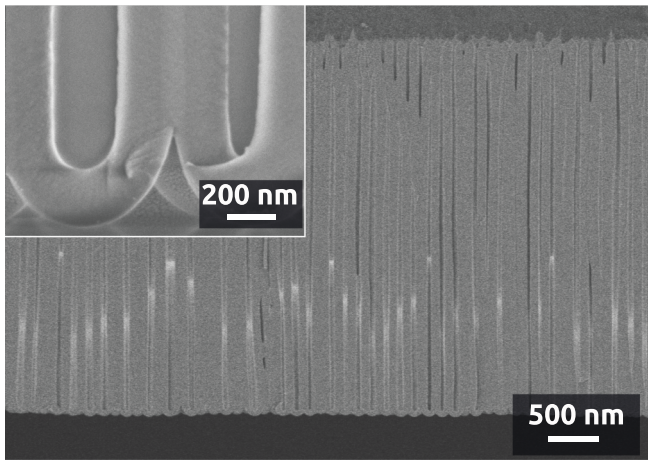


FIG. 13. Cross-sectional view of an alumina membrane grown in 0.05 M phosphoric acid under an applied potential of 195 V at 3 °C. The inset shows an enlarged view of the section of pores.

procedure described (with and without the final 5-min pore widening step). They are well organized on a large scale and the pore diameter is about 45 nm after pore widening (35 nm before it). A small fraction of pores are bifurcated near their opening. This phenomenon, which is observed to some extent in all anodizations, may be enhanced by the voltage ramp. All parts of the sample are similarly ordered, as shown in Fig. 10. The morphology of the pores is characterized in cross section in Fig. 11. They are straight on the whole depth of the membrane. They run parallel to each other, and their diameter is homogeneous from one extremity to the other.

### C. Anodization in phosphoric acid

Larger pores can be grown using a 0.05 M (0.5 wt. %) phosphoric acid solution under a voltage of 195 V. Note that the phosphoric acid concentration usually mentioned in the literature is 1 wt. %.[36] The lower concentration prevents pitting and results in a lower growth rate (about 1 $\mu$m/h) but yields a similar degree of order. The final applied voltage being higher

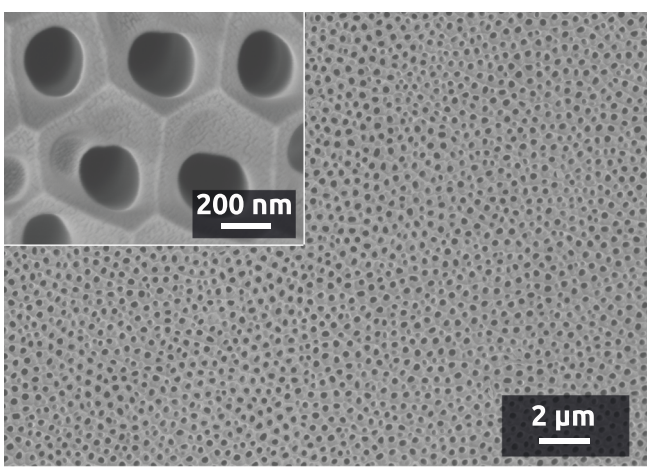


FIG. 12. Alumina membrane grown in 0.5% phosphoric acid under an applied potential of 195 V at 3 °C. The inset shows an enlarged view of the pores.

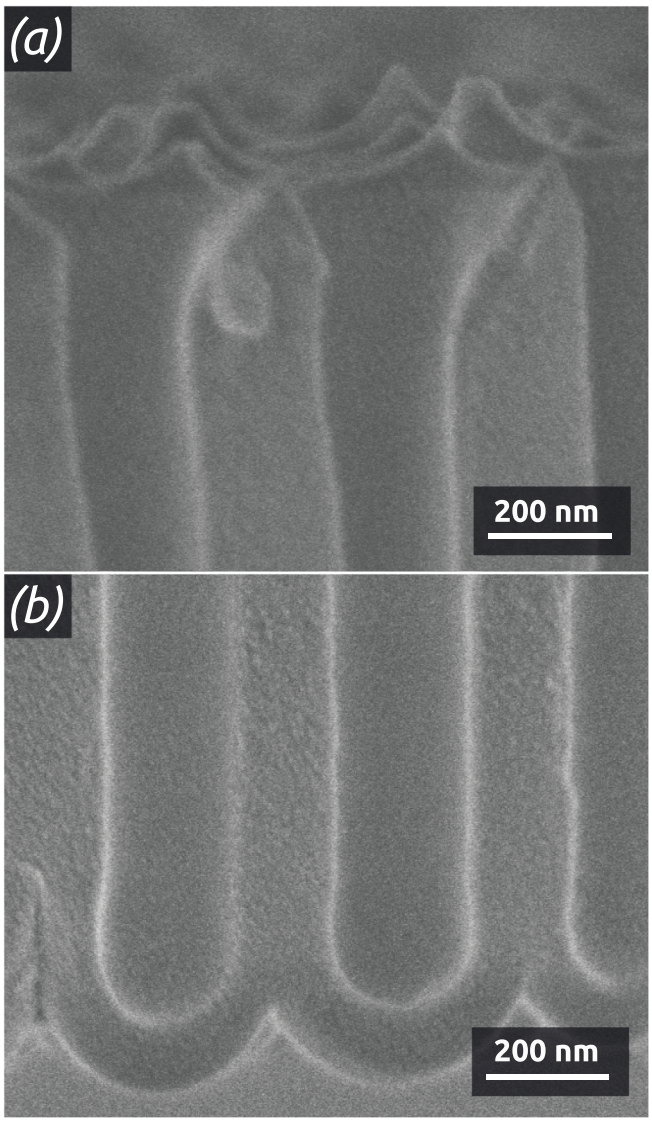


FIG. 14. Cross-sectional view of an alumina membrane grown in 0.5% phosphoric acid under an applied potential of 195 V at 3 °C. (a) Upper and (b) lower extremities of the pores.

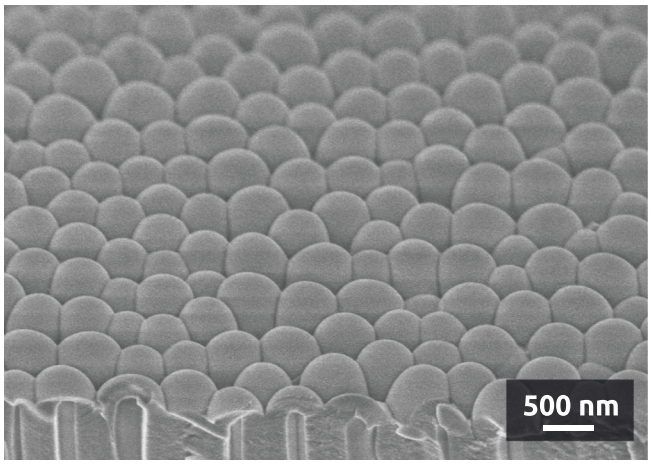


FIG. 15. Lower extremity of alumina pores grown in a phosphoric acid solution.

than in oxalic acid solution, the voltage ramp must also be slower, 0.1 V/s from 0 to 195 V. The voltage is then maintained for 24 h, and the current stabilizes at 120 mA. The temperature of both chillers cooling the electrolyte and the Cu electrode plate is set to 0 °C. At steady state, the temperature measured in the electrochemical cell is approximately 3 °C.

After the first anodization, the chemical dissolution of the alumina sacrificial layer is performed in the chromic acid solution as described above. For the second anodization, a ramp of 6 V/s is applied from 0 to 195 V. Again, we observe that a slower ramp leads to a poorer pore organization. However, the risk of pitting, materialized on the current-time trace example of Fig. 8(c) as a spike near 1000 s, defines the upper limit of the ramp rate. Note that if anodization is continued much beyond 3 h, the current will again decay slowly, as is always observed for phosphoric acid anodization.[19] Fig. 13 shows a top view of the alumina membranes with pores exhibiting a diameter of about 180(±40) nm. The inset shows an enlarged view of the pores. The pore diameter distribution shown in Fig. 8(b) yields 211(±18) nm as the 2σ interval of the best Gaussian fit, a value somewhat larger than typically reported in the literature (Table I).[30] However, the bar graph shows the presence of a significant fraction of small pores that are not apprehended by the Gaussian fit. In Fig. 12, they appear at faults in the ordered structure.

The cross section of the membrane is shown in Fig. 13. The pore length is about 3.5 $\mu$m for 4 h of anodization. The enlarged inset view displays the barrier oxide layer at the lower extremity of the pores. The pores exhibit the same diameter of about 180 nm at the upper and lower extremities as shown in Figs. 14(a) and 14(b), respectively. The lower extremity view of the pores (Fig. 15) reveals that the organization observed on the top side of the anodized membrane is found on its back side of the membrane, as well.

## V. CONCLUSIONS

We have established a setup and the associated procedures for making ordered arrays of cylindrical, parallel nanopores by anodizing aluminum in either oxalic acid or phosphoric acid. The samples feature a high degree of order over a surface of 200 cm$^2$, that is, a total of $10^{11}$ or $2 \times 10^{12}$ ordered pores per sample (for a pitch of 450 nm or 105 nm, respectively). In particular, the anodization in phosphoric acid under 195 V had only been performed on ≤10 cm$^2$ to date. The size increase by a factor of 20 has been made possible in this work by two features. The first is an extremely efficient cooling, obtained by combining the usual indirect cooling of the sample, on the one hand, with an additional direct cooling of the electrolyte, on the other hand. The second crucial aspect is the definition of voltage ramps at the start of the anodization procedure, which ensures a slow, controlled formation of the first oxide layer. Each of these features is precedented in the literature. However, their combination has never been published in the context of two-step anodization and is the enabler which eliminates what in many research groups used to be a bottleneck in the preparation of ordered, cylindrical anodic alumina pores of approximately 200 nm diameter: the maximal sample size.

Thus, the setup and procedures established here should facilitate the access to anodic alumina samples for the scientific community. Such samples can now be exploited as templates or substrates for applications in the catalysis, optics, biology, and energy storage realms and tested on a scale that goes beyond the academic setting.

## ACKNOWLEDGMENTS

We gratefully acknowledge M. Weller from the mechanical workshop (FAU Inorganic Chemistry) for his precious help building up the electrochemical cell. We thank Grisell Reyes Rios for performing some preliminary experiments, as well as the undergraduate students who contributed to the tests (F. Meyerhöfer, T. Bauer, M. Heilmann, D. Pividori, T. Reinhard, and H. Schlott). We acknowledge E. Butzen (MPI for the Science of Light) for his support with SEM. This work is funded by the project "tubulAir±" (Project No. 03SF0436G) supported by the Bundesministerium für Bildung und Forschung and by the DFG Cluster of Excellence "Engineering of Advanced Materials."

[1]A. Thormann, N. Teuscher, M. Pfannmöller, U. Rothe, and A. Heilmann, Small **3**, 1032 (2007).
[2]S. Ko, D. Lee, S. Jee, H. Park, K. Lee, and W. Hwang, Thin Solid Films **515**, 1932 (2006).
[3]G. K. Mor, O. K. Varghese, M. Paulose, K. Shankar, and C. A. Grimes, Sol. Energy Mater. Sol. Cells **90**, 2011 (2006).
[4]T. Kumeria, A. Santos, and D. Losic, Sensors **14**, 11878 (2014).
[5]L. Assaud, E. Monyoncho, K. Pitzschel, A. Allagui, M. Petit, M. Hanbücken, E. A. Baranova, and L. Santinacci, Beilstein J. Nanotechnol. **5**, 162 (2014).
[6]E. Moyen, L. Santinacci, L. Masson, H. Sahaf, M. Macé, L. Assaud, and M. Hanbücken, Int. J. Nanotechnol. **9**, 246 (2012).
[7]L. Assaud, K. Pitzschel, M. Hanbücken, and L. Santinacci, ECS J. Solid State Sci. Technol. **3**, P253 (2014).
[8]V. Roscher, M. Lickleder, J. Schumacher, G. Reyes Rios, B. Hoffmann, S. Christiansen, and J. Bachmann, Dalton Trans. **43**, 4345 (2014).
[9]T. Grünzel, Y. J. Lee, K. Kuepper, and J. Bachmann, Beilstein J. Nanotechnol. **4**, 655 (2013).
[10]J. Bachmann, J. Jing, M. Knez, S. Barth, H. Shen, S. Mathur, U. Gösele, and K. Nielsch, J. Am. Chem. Soc. **129**, 9554 (2007).
[11]P. Roy, S. Berger, and P. Schmuki, Angew. Chem., Int. Ed. **50**, 2904 (2011).
[12]W. Lee and S.-J. Park, Chem. Rev. **114**, 7487 (2014).
[13]K. Yasuda, J. M. Macak, S. Berger, A. Ghicov, and P. Schmuki, J. Electrochem. Soc. **154**, C472 (2007).

[14]Z. X. Su and W. Z. Zhou, Adv. Mater. **20**, 3663 (2008).
[15]Whatman "Anodisc" membranes are sold with a maximal area of 70 $cm^2$; SmartMembranes sells the "SmartPor" membranes with sizes up to 620 $cm^2$ grown in oxalic acid and 10 $cm^2$ grown in phosphoric acid.
[16]F. Keller, M. S. Hunter, and D. L. Robinson, J. Electrochem. Soc. **100**, 411 (1953).
[17]G. E. Thompson and G. C. Wood, Nature **290**, 230 (1981).
[18]H. Masuda and M. Satoh, Jpn. J. Appl. Phys., Part 2 **35**, L126 (1996).
[19]K. Nielsch, J. Choi, K. Schwirn, R. B. Wehrspohn, and U. Gösele, Nano Lett. **2**, 677 (2002).
[20]W. Lee, K. Schwirn, M. Steinhart, E. Pippel, R. Scholz, and U. Gösele, Nat. Nanotechnol. **3**, 234 (2008).
[21]W. Lee, K. Nielsch, and U. Gösele, Nanotechnology **18**, 475713 (2007).
[22]G. E. J. Poinern, N. Ali, and D. Fawcett, Materials **4**, 487 (2011).
[23]N. Itoh, K. Katob, T. Tsujib, and M. Hongob, J. Membr. Sci. **117**, 189 (1996).
[24]M. H. Miles and W. S. McEwan, J. Electrochem. Soc. **120**, 1069 (1973).
[25]A. M. M. Jani, D. Losic, and N. H. Voelcker, Prog. Mater. Sci. **58**, 636 (2013).
[26]C. Y. Han, G. A. Willing, Z. Xiao, and H. H. Wang, Langmuir **23**, 1564 (2007).
[27]O. Jessensky, F. Müller, and U. Gösele, Appl. Phys. Lett. **72**, 1173 (1998).
[28]E. Moyen, L. Santinacci, L. Masson, W. Wulfhekel, and M. Hanbücken, Adv. Mater. **24**, 5094 (2012).
[29]J. Oh and C. V. Thompson, Electrochim. Acta **56**, 4044 (2011).
[30]G. D. Sulka, in *Nanostructured Materials in Electrochemistry*, edited by A. Eftekhari (Wiley-VCH, Weinheim, Germany, 2008), Chap. 1.
[31]T. P. Hoar and N. F. Mott, J. Phys. Chem. Solids **9**, 97 (1959).
[32]J. P. O'sullivan and G. C. Wood, Proc. R. Soc. A **317**, 511 (1970).
[33]G. E. Thompson, Thin Solid Films **297**, 192 (1997).
[34]J. E. Houser and K. R. Hebert, Nat. Mater. **8**, 415 (2009).
[35]W. Lee, R. Ji, U. Gösele, and K. Nielsch, Nat. Mater. **5**, 741 (2006).
[36]H. Masuda, K. Yada, and A. Osaka, Jpn. J. Appl. Phys., Part 2 **37**, L1340 (1998).